Electronic Supplementary Information (ESI)

Sublimable cationic Ir(III) phosphor using chlorine as counterion for high-performance monochromatic and white OLEDs

Lei Ding,[a] Chun-Xiu Zang,[b] Hui-Ting Mao,[a] Guo-Gang Shan,*[a] Li-Li Wen,[a] Hai-Zhu Sun,*[a] Wen-Fa Xie,*[b] and Zhong-Min Su*[ac]

[a]*Institute of Functional Material Chemistry and National & Local United Engineering Lab for Power Battery, Faculty of Chemistry, Northeast Normal University, Changchun 130024, P. R. China*

Fax: +86-431-85684009Tel.: +86-431-85099108

E-mail:shangg187@nenu.edu.cn (G. Shan); sunhz335@nenu.edu.cn (H. Sun); zmsu@nenu.edu.cn (Z. Su)

[b] *State Key Laboratory on Integrated Optoelectronics, College of Electronic Science and Engineering, Jilin University, Changchun, Jilin 130012, P. R. China*

Tel: +86-13844907598, E-mail: xiewf@jlu.edu.cn (W. Xie)

[c] *School of Chemistry & Environmental Engineering, Changchun University of Science and Technology, Changchun, Jilin 130012, P. R. China*

Table of Contents

Experimental section

1. General information

All reagents and solvents were commercially available. Elemental analysis (C, H, and N) was determined on a Perkin-Elmer 240C elemental analyzer. [**(ptbi)$_2$Ir(bisq)**]**Cl**, [**(tbpbi)$_2$Ir(bisq)**]**Cl** and [**(tbpbi)$_2$Ir(bisq)**]**PF$_6$** were recorded by a ^{1}H NMR spectrum on Bruker Avance 600 MHz spectrometer, and chemical shifts are reported with tetramethylsilane (TMS) as the internal standard. The molecular weight of [**(ptbi)$_2$Ir(bisq)**]**Cl** was measured by using electrospray-ionization mass spectroscopy (ESI-MS).

2. Synthesis

The ancillary ligand 1-(1*H*-benzo[d]imidazol-2-yl)isoquinoline (Hbisq) was synthesized according to the previously reported literature with some modification.[1]

2.1. Synthesis of 1-phenyl-2-p-tolyl-1H-benzo[d]imidazole (ptbi)

50 mmol (9.21 g) of N-phenyl-o-phenylenediamine was dissolved in 30 mL of N, N-dimethylacetamide. Under nitrogen, 20 mL N, N-dimethylacetamide solution of 4-methylbenzoyl chloride (50 mmol, 7.73 g) was slowly added dropwise to above solution and stirred at room temperature for 1 h. After the reaction, a large amount of water was added to precipitate a solid. The solid was washed with methanol and water, then recrystallized with a mixed solution of N, N-dimethylacetamide and water. The resulting intermediate was added to 20 mL of glacial acetic acid and heated to reflux for 16 h, and then cooled to room temperature. Water was added to precipitate a solid and dried to give the product. Then, product was purified by column chromatography on silica gel. ^{1}H NMR (500 MHz, $CDCl_3$, δ): 7.89 (d, J = 8.0 Hz, 1H), 7.52-7.45 (m, 5H), 7.35-7.31 (m, 3H), 7.27-7.23 (m, 2H), 7.11 (d, J = 8.0 Hz, 2H), 2.34 (s, 3H).

2.2. Synthesis of dichloro-bridged diiridium complex

$[Ir(ptbi)_2Cl]_2$: $IrCl_3 \cdot 3H_2O$ (1.06 g, 3.00 mmol), ptbi (2.05 g, 7.20 mmol), 2-ethoxyethanol (60 mL) and water (20 mL) were mixed together and refluxed under argon for 24 hours. The reaction mixture was then cooled to room temperature and filtered. The product was washed with water and dried.

*2.3. Synthesis of complex **[(ptbi)$_2$Ir(bisq)]Cl***

The ancillary ligand Hbisq (0.15 g, 0.60 mmol) and the dichloro-bridged diiridium complex $[Ir(ptbi)_2Cl]_2$ (0.38 g, 0.24 mmol) are dissolved in dichloro-methane (30 mL) and ethanol (10 mL). Then the mixture was refluxed for 24 hours under the protection of light and argon. After cooling to room temperature, the mixture was distilled off the solvent and then the crude product was purified through silica gel column chromatography using an ethyl acetate-dichloromethane mixture (10 : 1) and then a dichloromethane-methanol mixture (25 : 1) as eluent to afford complex **[(ptbi)$_2$Ir(bisq)]Cl** in 68% yield. ^{1}H NMR (600 MHz, DMSO-d_6, δ): 10.79 (s, 1H), 8.05-8.07 (m, 2H), 7.71-7.93 (m, 12H), 7.58 (t, *J*=3.6 Hz, 2H), 7.45 (d, *J*=6.0 Hz, 1H), 6.95-7.10 (m, 5H), 6.81 (t, *J*=7.8 Hz, 1H), 6.73 (s, 1H), 6.69 (t, *J*=7.5 Hz, 1H), 6.49-6.58 (m, 4H), 6.37 (d, *J*=13.2 Hz, 2H), 6.26 (d, *J*=8.4 Hz, 1H), 5.83 (d, *J*=8.4 Hz,1H), 5.64 (d, *J*=4.8 Hz, 1H), 2.03 (d, *J*=9.0 Hz, 6H). MS (MALDI-TOF): m/z 1004.3.

2.4. Synthesis of complex ***[(tbpbi)$_2$Ir(bisq)]Cl***

The synthetic method of **[(tbpbi)$_2$Ir(bisq)]Cl** is similar to that of **[(ptbi)$_2$Ir(bisq)]Cl**, in which the dichloro-bridged diiridium complex $[Ir(ptbi)_2Cl]_2$ is replaced by $[Ir(tbpbi)_2Cl]_2$.

[(tbpbi)$_2$Ir(bisq)]Cl in 67% yield. ^{1}H NMR (600 MHz, DMSO-d_6, δ): 10.86 (s, 1H), 8.05 (d, *J*=7.2 Hz, 1H), 7.98 (d, *J*=6.0 Hz, 1H), 7.92-7.94 (m, 2H), 7.70-7.85 (m, 11H), 7.27-7.32 (m, 2H), 7.14-7.15 (m, 1H), 7.06-7.09 (m, 2H), 6.99 (d, *J*=8.4 Hz, 2H), 6.91 (t, *J*=7.8 Hz, 1H), 6.79-6.81 (m, 1H), 6.75-6.76 (m, 1H), 6.72 (t, *J*=7.8 Hz, 1H), 6.58-6.60 (m, 2H), 6.47-6.52 (m, 3H), 5.97-6.00 (m, 2H), 5.75-5.76 (m, 1H), 0.89 (d, J=7.2Hz, 18H)

2.5. Synthesis of complex ***[(tbpbi)$_2$Ir(bisq)]PF$_6$***

The ancillary ligand Hbisq (0.15 g, 0.60 mmol) and the dichloro-bridged diiridium complex $[Ir(tbpbi)_2Cl]_2$ (0.42 g, 0.24 mmol) are dissolved in dichloro-methane (30 mL) and ethanol (10 mL). Then the mixture was refluxed for 24 hours under the protection of light and argon. After cooling to room temperature, an aqueous solution of KPF_6 was slowly added into the reaction mixture under stirring. The crude product was purified by column chromatography on silica gel with dichloromethane- methanol (v/v = 10:1) as the eluent.

[(tbpbi)$_2$Ir(bisq)]PF$_6$ in 65% yield. ^{1}H NMR (600 MHz, DMSO-d_6, δ): 15.11 (s, 1H), 8.22 (s, 1H), 8.08 (t, *J*=7.8 Hz, 4H), 7.86 (d, *J*=7.2 Hz, 1H), 7.75-7.82 (m, 8H), 7.70 (d, *J*=7.8 Hz, 1H), 7.32-7.33 (m, 2H), 7.27-7.28 (m, 1H), 7.18 (t, *J*=7.8 Hz, 1H), 7.14 (t, *J*=7.8 Hz, 1H), 7.09 (d, *J*=7.8 Hz, 1H), 7.05 (d, *J*=8.4 Hz, 1H), 6.93 (t, *J*=7.8 Hz, 2H), 6.81-6.88 (m, 3H), 6.55 (d, *J*=1.8 Hz, 1H), 6.50 (t, *J*=8.7 Hz, 2H), 6.44 (s, 1H), 6.13 (d, *J*=7.8 Hz, 1H), 5.90 (t, *J*=9.9 Hz, 2H), 0.88 (s, 18H)

3. Physical measurements

The UV-vis absorption spectrum was measured on a Cary 500 UV-vis-NIR spectrophotometer. Emission spectra of **[(ptbi)$_2$Ir(bisq)]Cl** was recorded on the FL-4600 FL spectrophotometer at room temperature. The neat film was prepared through spin-coating a solution of **[(ptbi)$_2$Ir(bisq)]Cl** in CH_3CN (20 mg mL^{-1}) on precleaned glass substrates at 2000 rpm. Then, PLQY (Φ_p) in a neat film was performed on an integrating sphere in a fluorospectrophotometer. The excited-state lifetime and PLQY in solution were measured on a transient spectrofluorimeter (EdinburghFLSP920) using a time-correlated single-photon counting technique. The thermogravimetric analysis was performed on a Perkin-Elmer TG-7 analyzer heated from 30 to 800 °C in a nitrogen atmosphere at a scanning rate of 10 °C min^{-1}. The differential scanning calorimetry analysis was measured on a NETZSCH DSC-204 analyzer heated from 30 to 400 °C in a nitrogen atmosphere at a scanning rate of 10 °C min^{-1}.

4. Theoretical Calculation.

Theoretical Calculation on **[(ptbi)$_2$Ir(bisq)]Cl** was performed by Gaussian 09 software package.[2] The structure of iridium(III) complex was fully optimized with PBE0 for ground states (S_0) geometry and spin-unrestricted open-shell PBE0 for the lowest triplet state (T_1) geometry, respectively. The standard 6-31G** basis set was used C, H and N atoms, and the LANL2DZ on the iridium(III) atom was employed in all calculations. To assist in understanding the excited-state electronic properties of **[(ptbi)$_2$Ir(bisq)]Cl**, the time-dependent density functional theory (TDDFT) calculation was employed considering the implicit acetonitrile solvent effect.

5. Cyclic voltammetry

Cyclic voltammetry was recorded on a BAS 100 W instrument with a scan rate of 100 mV s^{-1} in CH_3CN (10^{-3} M) with three-electrode conguration: a glassy carbon electrode as the working electrode, an aqueous saturated calomel electrode as the operating reference electrode and a platinum wire as the counter electrode. A 0.1 M solution of tetra-butylammonium tetrafluoroborate in CH_3CN was used as the supporting electrolyte and ferrocene was selected as the internal standard.

6. Device fabrication and characterization

Patterned indium-tin-oxide (ITO)-coated glass substrates with the sheet resistance of 20 Ω per square were cleaned with rinsing in Decon 90, deionized water, drying in an oven, and finally were treated in a UV-ozone chamber. Organic layers and cathode were sequentially deposited on the ITO-glass substrates without breaking the vacuum (~5.0×10^{-4} Pa). [**(ptbi)$_2$Ir(bisq)**]**Cl** was sequentially deposited on the ITO-glass substrates without breaking the vacuum (~5.0×10^{-4} Pa) and keeping 220 °C. A shadow mask was used to define the cathode and to make four 10 mm^2 devices on each substrate. The thickness of the organic layers and metal were monitored in situ with quartz oscillator. Luminance–current–voltage characteristics of the unpackaged devices were measured simultaneously with a programmable Keithley 2400 source meter and a Minolta luminance meter LS-110. The spectra of the devices were measured with an Ocean Optics Maya 2000-PRO spectrometer. All the measurements were carried out at room temperature in air.

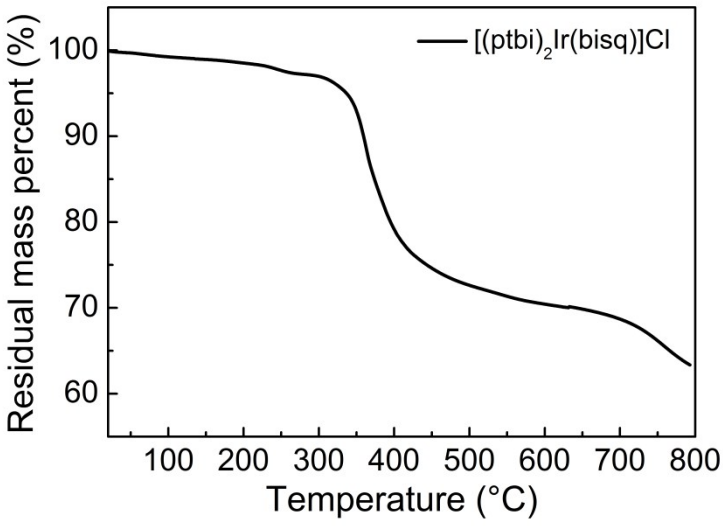

Fig. S1 Thermal gravimetric analysis (TGA) curves of **[(ptbi)$_2$Ir(bisq)]Cl** under a dry nitrogen gas flow at a heating rate of 10°C min^{-1}.

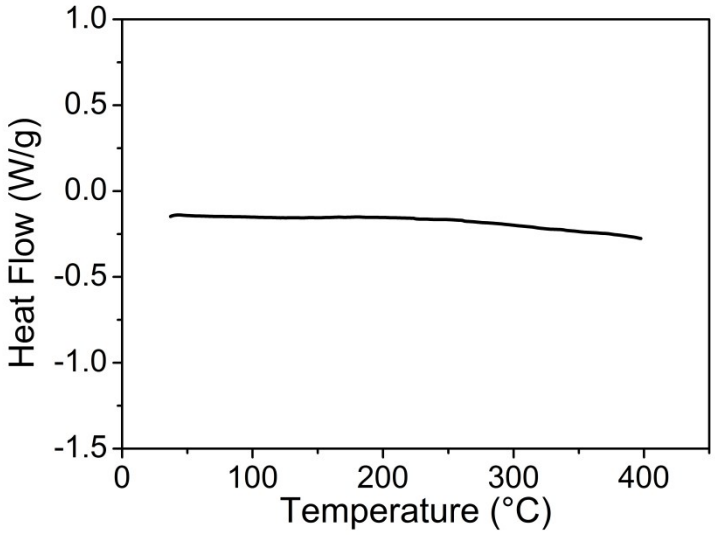

Fig. S2 The second cycle differential scanning calorimetry (DSC) curves of **[(ptbi)$_2$Ir(bisq)]Cl** under a dry nitrogen gas flow at a heating rate of 10°C min^{-1}.

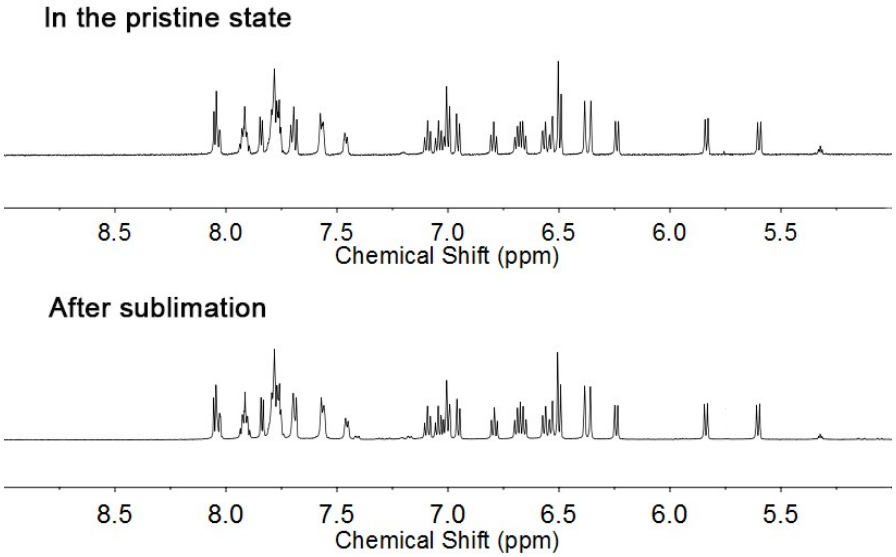

Fig. S3 ^{1}H NMR spectra of **[(ptbi)$_2$Ir(bisq)]Cl** in the pristine state and after sublimation.

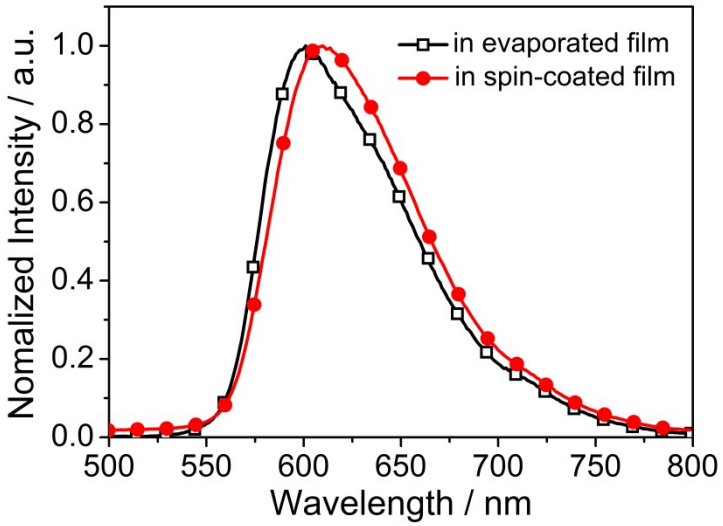

Fig. S4 PL spectra of [**(ptbi)$_2$Ir(bisq)]Cl** in spin-coated and vacuum-evaporated film.

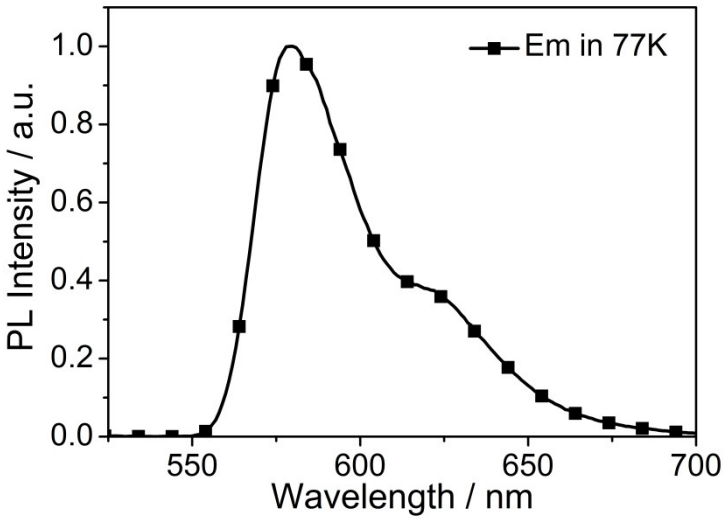

Fig. S5 PL spectra of [**(ptbi)$_2$Ir(bisq)]Cl** in 77 K.

Table S1. Photophysical and electrochemical characteristics for [**(ptbi)$_2$Ir(bisq)]Cl**

Complex	$\lambda_{PL,max}$ [a),b),c)] [nm]	ϕ_p [a),c)] [%]	τ [a),c)] [μs]	E_{ox} [d)] [V]	E_g [e)] [eV]	HOMO [f)] [eV]	LUMO [g)] [eV]	k_r [a), c)] [10^5 s^{-1}]	k_{nr} [a), c)] [10^5 s^{-1}]
[(ptbi)$_2$Ir(bisq)]Cl	608, 580, 610	17.8, 32.4	0.67, 0.86	0.37	2.34	–5.17	–2.83	2.66, 3.77	12.27, 7.86

[a] Measured in acetonitrile (10^{-5} M) at 298 K. [b] 77 K. [c] Measured in the neat film. [d] Measured by CV with ferrocene as the standard. [e] Estimated from the UV-vis absorption spectrum. [f] Calculated from onset oxidation potential. [g] Deduced from HOMO and Eg

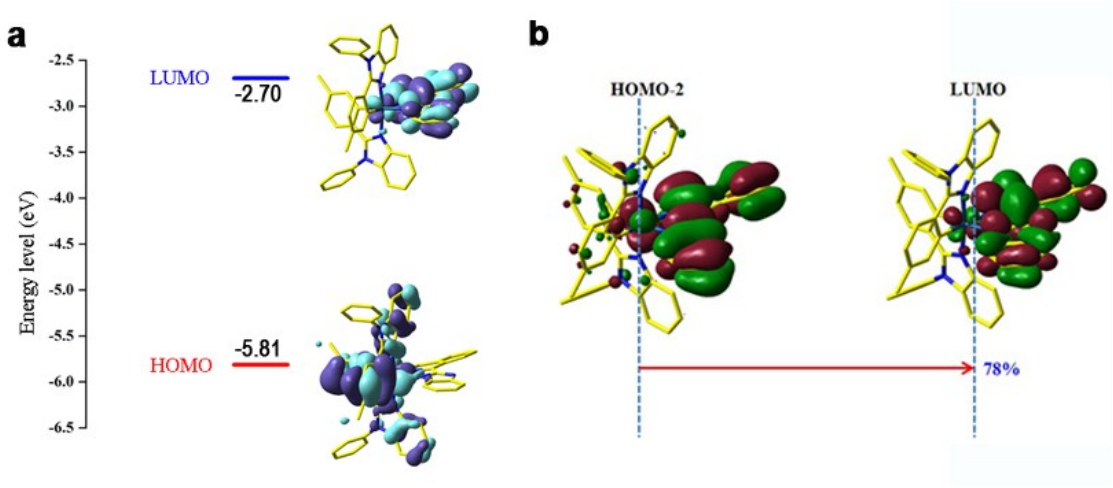

Fig. S6 (a) Calculated HOMO and LUMO levels and distributions of **[(ptbi)$_2$Ir(bisq)]Cl**. All MO surfaces correspond to an isocontour value of $|\Psi| = 0.02$. (b) Orbital transition analyses of T_1 state for **[(ptbi)$_2$Ir(bisq)]Cl**.

Table S2. Calculated triplet excited energy, and transition characteristic of T_1 state for **[(ptbi)$_2$Ir(bisq)]Cl**

Complex	State	eV	Assignment	Character
[(ptbi)$_2$Ir(bisq)]Cl	T_1	1.929	HOMO-2→LUMO（78%）	^{3}MLCT/^{3}LLCT

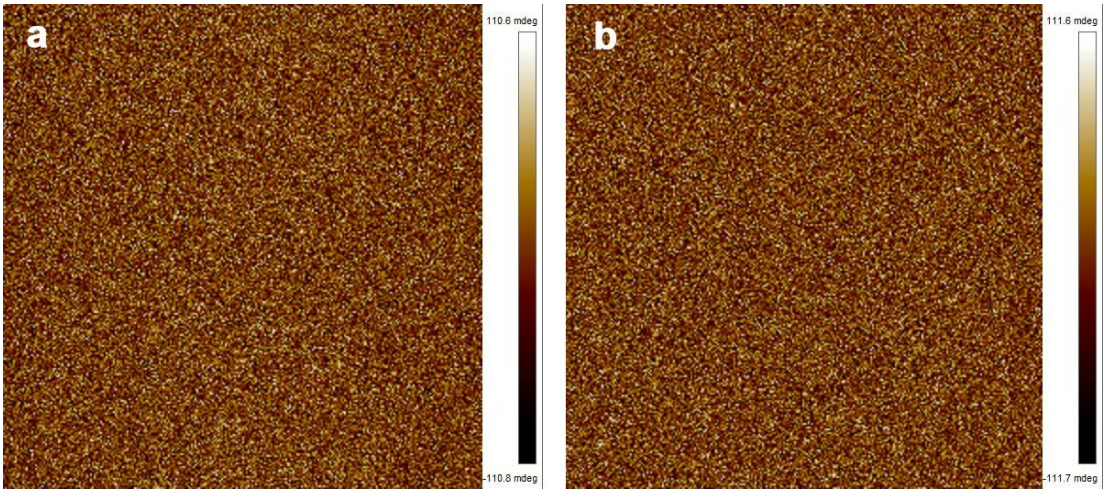

Fig. S7 AFM images of (a) non-doped evaporated film and (b) doped evaporated film.

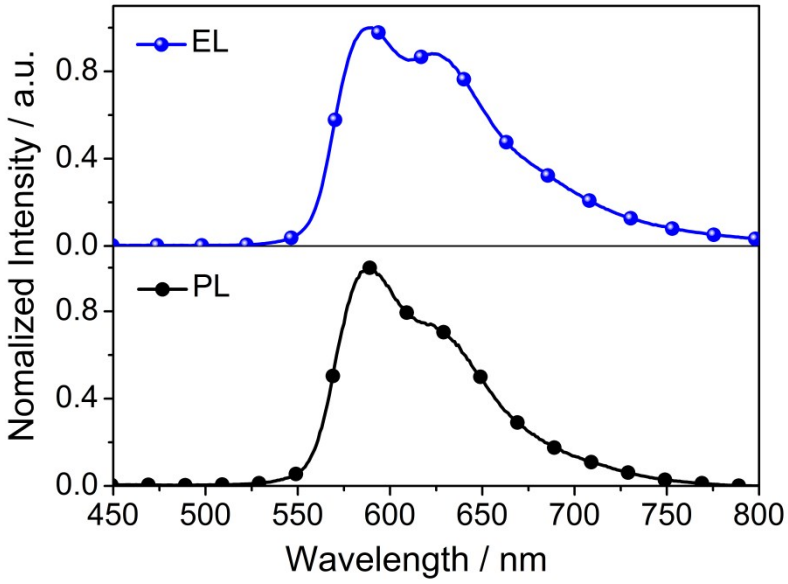

Fig. S8 PL in the co-evaporated film and EL spectra in doped device.

Table S3. Monochromatic OLEDs performance of selected cationic Ir(III) complexes

complex	host	λ_{EL} [nm]	$V_{turn\text{-}on}$ [V]	Max CE [cd A^{-1}]	Max PE [lm W^{-1}]	Max EQE [%]	L_{max} [b)] [cd m^{-2}]	CIE[(x, y)]	Ref
[(ptbi)$_2$Ir(bisq)]Cl	DCZppy	590, 624	3.3	17.8	15.4	10.5	25035	(0.60, 0.40)	This work
[Ir(dpfd)$_2$(dmbpy)][PF_6]	CBP	565	5.0	19.7	18.4	6.5	15611	(0.44, 0.47)	3
[Ir(ppy)$_2$(ECAF)][PF_6]	CBP	540	9.2	20.2	4.9	6.3	8588	(0.38, 0.58)	4

$[Ir(ppy)_2(EHCAF)][PF_6]$	CBP	540	8.4	23.7	5.3	6.8	11850	(0.37, 0.58)	4
$[Ir(ppy)_2(PCAF)][PF_6]$	CBP	540	8.2	21.5	5.6	6.5	10340	(0.38, 0.58)	4
$[Ir(dfppy)_2(pzpy)][B(5fph)_4]$	$CzPO_2$	452	7.0	1.5	0.4	1.5	5700	(0.18, 0.19)	5
$[Ir(dfppy)_2(pzpy)][BArF_{24}]$	$CzPO_2$	452	8.7	1.2	0.4	1.2	4400	(0.17, 0.17)	5
$[Ir(ppy)_2(pyim)][B(5fph)_4]$	DIC-TRZ	532	4.9	15.3	8.3	5.0	>27100	(0.35, 0.57)	5
$[Ir(ppy)_2(pyim)][BArF_{24}]$	DIC-TRZ	532	4.3	16.3	10.5	5.3	>27100	(0.36, 0.57)	5
$[Ir(ppy)_2(bpy)][B(5fph)_4]$	DIC-TRZ	550	4.4	24.3	12.9	8.1	>27100	(0.42, 0.54)	5
$[Ir(ppy)_2(bpy)][BArF_{24}]$	DIC-TRZ	551	3.4	22.6	15.4	7.5	>27100	(0.42, 0.54)	5
$[Ir(ppy)_2(ptop)][B(5fph)_4]$	DIC-TRZ	588	5.4	4.5	1.5	1.6	22100	(0.51, 0.47)	5
$[Ir(ppy)_2(ptop)][BArF_{24}]$	DIC-TRZ	588	5.6	7.1	2.8	2.5	16300	(0.52, 0.46)	5
$[Ir(ppy)_2(pop)][B(5fph)_4]$	DIC-TRZ	596	5.7	4.5	/	2.2	19400	(0.52, 0.46)	6
$[Ir(ppy)_2(pop)][B(5fph)_4]$	TCTA	592	6.9	3.4	/	1.8	4400	(0.52, 0.45)	6
$[Ir(ppy)_2(pop)][BArF_{24}]$	DIC-TRZ	596	5.6	5.1	/	2.5	11100	(0.52, 0.46)	6
$[Ir(ppy)_2(pop)][BArF_{24}]$	TCTA	596	5.1	2.8	/	1.4	4600	(0.50, 0.44)	6
$[Ir(dFppy)_2(Phpybi)][B(5FPh)_4]$	DIC-TRZ	521, 552	2.6	28.6	23.5	10.0	>27300	(0.41, 0.55)	7
$[Ir(dFppy)_2(Phpybi)][B(dCF_3Ph)_4]$	DIC-TRZ	520, 550	2.4	33.6	31.6	10.9	>27300	(0.39, 0.56)	7
$[Ir(piq)_2(Phpybi)][B(5FPh)_4]$	DIC-TRZ	588, 626	2.4	17.4	14.9	11.1	>27300	(0.60, 0.40)	7
$[Ir(piq)_2(Phpybi)][B(dCF_3Ph)_4]$	DIC-TRZ	588, 624	2.5	18.2	15.9	11.0	20500	(0.59, 0.40)	7
$[Ir(phq)_2(bpy)][B(5FPh)_4]$	DIC-TRZ	556, 591	2.2	33.1	32.2	11.1	>27300	(0.47, 0.51)	8
$[Ir(phq)_2(bpy)][B(dCF_3Ph)_4]$	DIC-TRZ	560, 589	2.5	37.0	37.5	13.7	>27300	(0.48, 0.51)	8
$[Ir(piq)_2(bpy)][B(5FPh)_4]$	DIC-TRZ	588, 624	2.2	16.8	18.1	10.3	>27300	(0.59, 0.40)	8
$[Ir(piq)_2(bpy)][B(dCF_3Ph)_4]$	DIC-TRZ	588, 624	2.4	16.4	14.2	9.9	>27300	(0.59, 0.40)	8
$[Ir(ppy)_2(pzpy)]$ $[B(5FPh)_4]$	DMAC-DPS	510	2.6	27.9	23.4	10.5	22640	(0.28, 0.55)	9
$[Ir(ppy)_2(pzpy)][B(dCF_3Ph)_4]$	DMAC-DPS	482, 506	3.0	24.5	21.5	9.8	11480	(0.21, 0.44)	9
$[Ir(ppy)_2(dtb\text{-}bpy)][B(5FPh)_4]$	DIC-TRZ	556	2.3	46.5	37.9	14.8	>27300	(0.43, 0.55)	10
$[Ir(ppy)_2(dtb\text{-}bpy)][B(dCF_3Ph)_4]$	DIC-TRZ	564	2.5	40.7	31.8	13.5	>27300	(0.44, 0.53)	10
$[Ir(phq)_2(dtb\text{-}bpy)][B(5FPh)_4]$	DIC-TRZ	556, 586	2.2	40.6	40.9	13.8	>27300	(0.48, 0.51)	10
$[Ir(phq)_2(dtb\text{-}bpy)][B(dCF_3Ph)_4]$	DIC-TRZ	558, 586	2.3	48.9	49.0	15.8	>27300	(0.48, 0.51)	10
$[Ir(piq)_2(dtb\text{-}bpy)][B(5FPh)_4]$	DIC-TRZ	588, 626	2.4	16.5	16.6	10.7	>27300	(0.60, 0.40)	10
$[Ir(piq)_2(dtb\text{-}bpy)][B(dCF_3Ph)_4]$	DIC-TRZ	588, 624	2.4	18.0	19.1	11.1	18800	(0.59, 0.40)	10

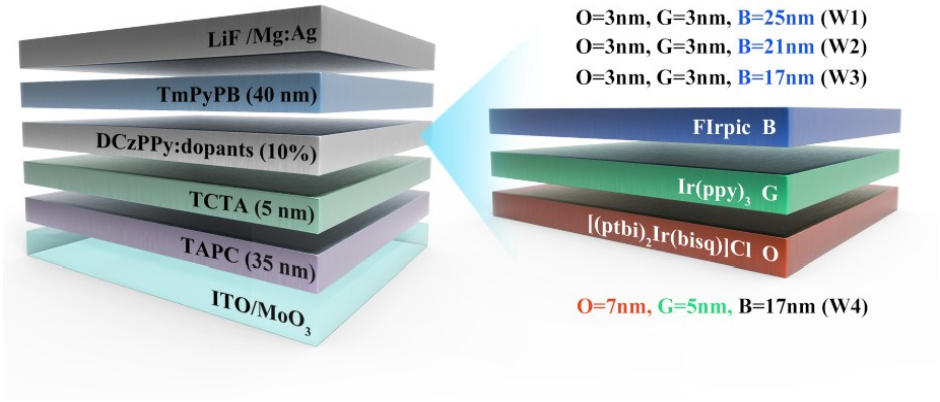

Fig. S9 Schematic diagram of white OLEDs optimization process

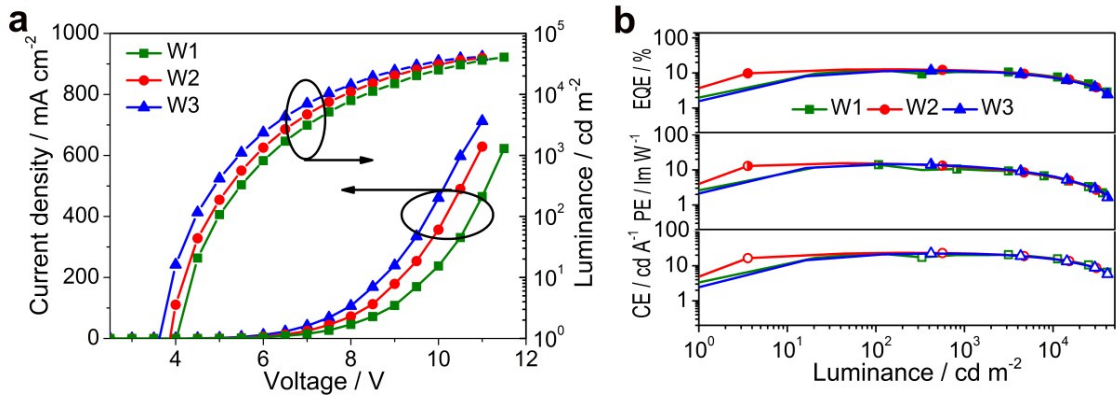

Fig. S10 (a) Current density-voltage-luminance (b) Current, Power, and external quantum efficiency curves for **W1-W3**.

Table S4. Summary of electroluminescence performances for W1-W3

Device	$V_{turn\text{-}on}$ [a)] [V]	CE [b), c)] [cd A^{-1}]	PE [b), c)] [lm W^{-1}]	EQE [b)] [%]	Efficiency roll-offs [%]			L_{max} [b)] [cd m^{-2}]	CIE[(x, y)]	CRI
					CE	PE	EQE			
W1	4.0	22.4/20.2	14.1/10.4	12.3/10.6	9.8	26	13.6	40786	(0.48,0.42)	80
W2	3.6	23.4/22.7	15.6/12.2	12.5/11.8	3.0	22	6.0	39712	(0.48,0.42)	80
W3	3.5	22.5/21.9	14.6/12.7	11.6/11.2	2.7	13	3.6	41358	(0.48,0.42)	80

[a)] Defined as the bias at a brightness of 1 cd m^{-2} . [b)] Maximum values of the devices. [c)] Values of the devices at 1000 cd m^{-2}

Table S5. WOLEDs performance of selected cationic iridium(III) complexes

Device	$V_{turn\text{-}on}$ [V]	Max CE [cd A^{-1}]	Max PE [lm W^{-1}]	Max EQE [%]	L_{max} [cd m^{-2}]	CIE[(x, y)]	CRI	Ref
1	5.4	1.8	/	0.9	3700	(0.33,0.34)	86	4
2	6.0	0.5	/	0.4	1900	(0.32,0.27)	89	4
W1	4.0	22.4	14.1	12.3	40786	(0.48,0.42)	80	This work
W2	3.6	23.4	15.6	12.5	39712	(0.48,0.42)	80	This work
W3	3.5	22.5	14.6	11.6	41358	(0.48,0.43)	80	This work
W4	3.6	25.5	17.3	13.1	50122	(0.49,0.45)	80	This work

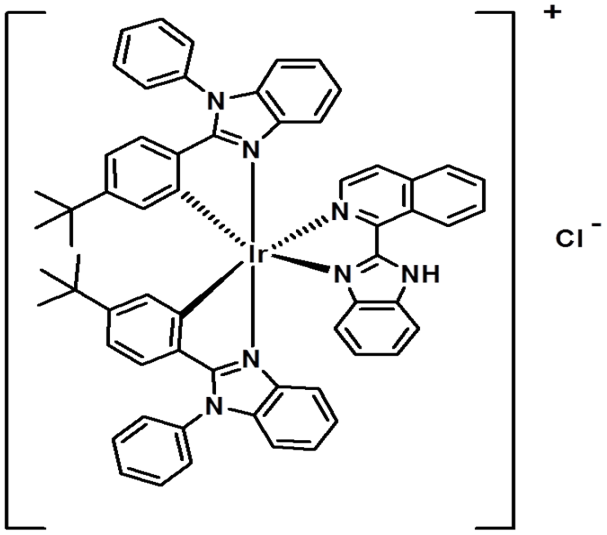

Fig. S11 Chemical structure of [**(tbpbi)$_2$Ir(bisq)**]**Cl**.

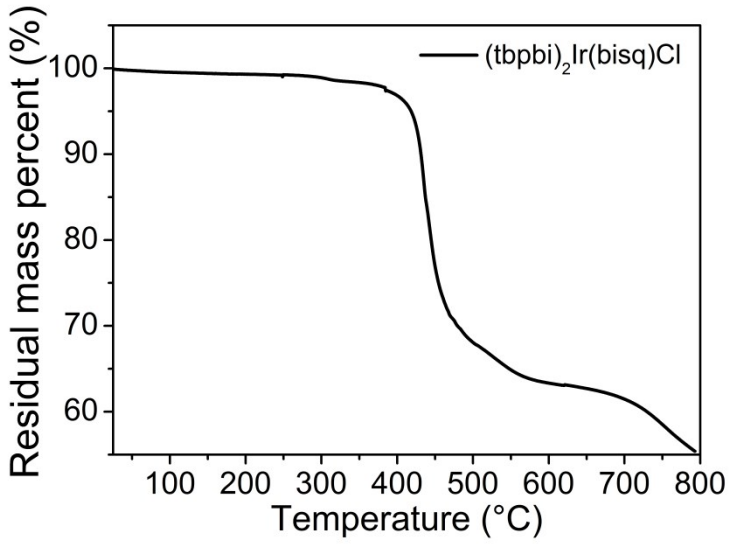

Fig. S12 Thermal gravimetric analysis (TGA) curves of **[(tbpbi)$_2$Ir(bisq)]Cl** under a dry nitrogen gas flow at a heating rate of 10°C min^{-1}.

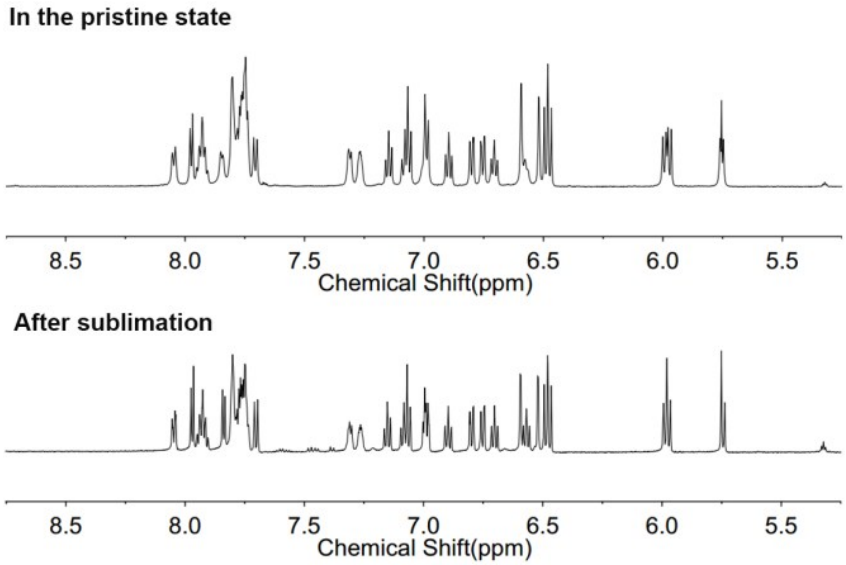

Fig. S13 ^{1}H NMR spectra of **[(tbpbi)$_2$Ir(bisq)]Cl** in the pristine state and after sublimation.

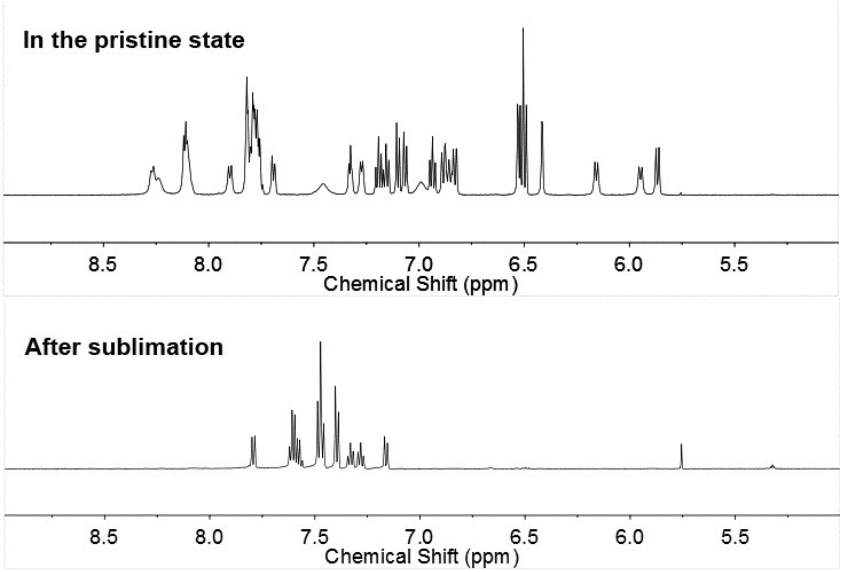

Fig. S14 ^{1}H NMR spectra of $[(\mathbf{tbpbi})_2\mathbf{Ir}(\mathbf{bisq})]\mathbf{PF_6}$ in the pristine state and after sublimation.

References

1. T.-R. Chen, *Mater. Lett.*, 2005, **59**, 1050.

2 Frisch, M. J.; Trucks, G. W.; Schlegel, H. B.; Scuseria, G. E.; Robb, M. A.; Cheeseman, J. R.; Scalmani, G.; Barone, V.; Mennucci,B.; Petersson, G. A.; Nakatsuji, H.; Caricato, M.; Li, X.; Hratchian, H. P.; Izmaylov, A. F.; Bloino, J.; Zheng, G.; Sonnenberg, J. L.; Hada, M.; Ehara, M.; Toyota, K.; Fukuda, R.; Hasegawa, J.; Ishida, M.; Nakajima, T.; Honda, Y.; Kitao, O.; Nakai, H.; Vreven, T.; Montgomery, J. A., Jr.; Peralta, J. E.; Ogliaro, F.; Bearpark, M.; Heyd, J. J.; Brothers, E.; Kudin, K. N.; Staroverov, V. N.; Kobayashi, R.; Normand, J.; Raghavachari, K.; Rendell, A.; Burant, J. C.; Iyengar, S. S.; Tomasi, J.; Cossi, M.; Rega, N.; Millam, J. M.; Klene, M.; Knox, J. E.; Cross, J. B.; Bakken, V.; Adamo, C.; Jaramillo, J.; Gomperts, R.; Stratmann, R. E.; Yazyev, O.; Austin, A. J.; Cammi, R.; Pomelli, C.; Ochterski, J. W.; Martin, R. L.; Morokuma, K.; Zakrzewski, V. G.; Voth, G. A.; Salvador, P.; Dannenberg,

J. J.; Dapprich, S.; Daniels, A. D.; Farkas, Ö .; Foresman, J. B.; Ortiz, J. V.; Cioslowski, J.; Fox, D. J. Gaussian 09, Revision D.01; Gaussian, Inc.: Wallingford, CT, 2013.

3. W. Y. Wong, G. J. Zhou, X. M. Yu, H. S. Kwok and Z. Lin, *Adv. Funct. Mater.*, 2007, **17**, 315.
4. F. Zhang, Y. Guan, S. Wang, S. Li, F. Zhang, Y. Feng, S. Chen, G. Cao and B. Zhai, *Dyes Pigments*, 2016, **130**, 1.
5. D. Ma, Y. Qiu and L. Duan, *Adv. Funct. Mater.*, 2016, **26**, 3438.
6. D. Ma, L. Duan and Y. Qiu, *J. Mater. Chem. C*, 2016, **4**, 5051.
7. D. Ma, C. Zhang, R. Liu, Y. Qiu and L. Duan, *Chem.Eur.J.*, 2018, **24**, 5574.
8. D. Ma, R. Liu, Y. Qiu and L. Duan, *J. Mater. Chem. C*, 2018, **6**, 5630.
9. D. Ma, Y. Qiu and L. Duan, *ChemPlusChem*, 2018, **83**, 211.
10. D. Ma, R. Liu, C. Zhang, Y. Qiu, L. Duan, *ACS Photonics* **2018**, DOI: 10.1021/acsphotonics.8b00716.